Interplay between Local Diffusion, Concentration, and Inter-Protein Alignment Promotes Cross-β-Sheet Transitions at Condensate Interfaces

Alejandro Castro[1], Juan Luengo-Márquez[1], Andres R. Tejedor[1,2], Rosana Collepardo-Guevara[2,3,4,5], Marcell Papp[6], Paolo Arosio[6], Alberto Ocaña[5,7,8], Ignacio Sanchez-Burgos[2,3*] and Jorge R. Espinosa[1,2,3,5,8*]

[1] Department of Physical-Chemistry, Universidad Complutense de Madrid, Av. Complutense s/n, 28040, Madrid, Spain.
[2] Yusuf Hamied Department of Chemistry, University of Cambridge, Lensfield Road, Cambridge CB2 1EW, United Kingdom
[3] Maxwell Centre, Cavendish Laboratory, Department of Physics, University of Cambridge, J J Thomson Avenue, Cambridge CB3 0HE, United Kingdom.
[4] Department of Genetics, University of Cambridge, Cambridge CB2 3EH, United Kingdom.
[5] PhAsIca Biosciences S.L, Calle Velázquez, 27, 28001 Madrid, Spain
[6] Institute of Biochemistry, Department of Biology, ETH Zurich, Zurich, 8093, Switzerland
[7] Experimental Therapeutics in Cancer Unit, Instituto de Investigación Sanitaria San Carlos (IdISSC), and CIBERONC, Madrid, Spain
[8] Multidisciplinary Institute, Complutense University of Madrid, Paseo Juan XXIII, 1, Madrid 28040, Spain
** = To whom correspondence should be sent. email: is490@cam.ac.uk, jorgerene@ucm.es*

(Dated: March 5, 2026)

Biomolecular condensates govern cellular organization through dynamic, membraneless compartments whose material properties are dictated by intermolecular interactions. While liquid–liquid phase separation enables reversible condensate self-assembly, its dysregulation can trigger the formation of pathological solid-like states, often associated with neurodegenerative disorders. Here, we investigate the molecular mechanisms underlying condensate solidification, focusing on the role of inter-protein β-sheet transitions. Using a minimal protein coarse-grained model, we reveal that the condensate's interface acts as a hotspot for inter-protein β-sheet nucleation and growth. Residue- and segment-resolved analyses show that enhanced interfacial mobility, particularly of terminal domains, coupled with locally high protein concentrations, creates optimal conditions for inter-protein β-sheet-sheet formation. Moreover, favourable inter-protein orientational alignment of terminal domains emerges at the interface. We find that asymmetric sequences—e.g. those with defined hydrophobic vs. more hydrophilic regions—further amplify this effect, resulting in local density fluctuations which concentrate aggregation-prone domains at the interface, and collectively promote inter-protein β-sheet transitions. Such amphiphilic interfacial organization is driven by surface-tension minimization, and stabilizes protein structural rearrangements accentuating the spatial bias of inter-protein structural transitions. Altogether, our results demonstrate that general protein polymer-physics models, capturing only essential features such as flexibility and sequence patterning, inherently display condensate solidification at the interface. These findings identify the interface as a central regulator of condensate hardening, linking molecular-scale interactions to mesoscale phase behaviour, and providing mechanistic insight into the spatiotemporal onset of protein dysregulation in membraneless organelles.

I. INTRODUCTION

Cells achieve spatiotemporal compartmentalization and biological function through the formation of highly coordinated and specialized organelles[1]. This organization enables precise control over the diverse biochemical reactions occurring within the cell, and it is essential for regulating cellular activity[2]. Organelles are generally classified into two types: membrane-bound organelles, which have been extensively investigated[3], and membraneless organelles, whose properties are still being elucidated[4,5]. The latter, also known as biomolecular condensates[2,6], are ubiquitous within cells. Prominent examples include stress granules, which modulate stress responses, antiviral defence, and signalling pathways by concentrating mRNAs and proteins[7]; nuclear bodies such as the nucleolus[8–10], where ribosomal RNA is synthesized; or Cajal bodies, which are involved in snRNP maturation[2,11] among others. The functional relevance of biomolecular condensates arises from their ability to dynamically assemble and disassemble, providing a highly tunable mechanism for regulating cellular processes and enable precise spatiotemporal control of cellular organization and function.[12–14].

Condensates are primarily formed through phase-separation of proteins, nucleic acids, and other macromolecules which exhibit multivalent and dynamic transient interactions[2,15]. Among these components, RNAs play a central role in mediating phase-separation through specific (e.g., protein RNA-binding domains) and non-specific (i.e., electrostatic forces or π-π stacking) protein–RNA interactions[8,16–18]. These interactions are often complemented by protein low-complexity domains (LCDs)[6,19,20], which predominantly engage in multiple intermolecular weak protein–protein interactions. Condensate formation is highly sensitive to thermodynamic conditions[21], and it can be subtly modulated by changes in the cellular environment, such as temperature[22], salt concentration[23], or pH[24,25] among other multiple factors. This delicate balance renders phase-separation susceptible to regulatory failures, which can promote the formation of aberrant solid-like

structures associated with the onset of different neurodegenerative disorders[26,27]. Notable examples include amyotrophic lateral sclerosis (ALS), in which sequence-specific mutations alter the phase behaviour of RNA/DNA-binding proteins proteins such as the transactive response DNA-binding protein of 43 kDa (TDP-43) and fused in sarcoma (FUS)[28–31]; Parkinson's disease, linked to α-synuclein aberrant fibrillation[32]; and several forms of dementia, where Tau protein misfolding and aggregation generate cytotoxic assemblies[33–35].

The transition from a functional liquid-like (soluble) condensate to a pathological solid-like (insoluble) state (i.e. usually termed as ageing) involves the emergence of structural inter-protein transitions giving rise to cross-β-sheet motifs[36]. The progressive formation, and accumulation, of inter-protein cross-β-sheets within condensates is tightly linked to changes in material properties[37], with condensates transitioning from liquid-like behaviour—characterized by transient interactions—to solid-like, kinetically trapped states[38]. One evident manifestation of this transformation as a consequence of the intermolecular network strengthening is the reduction in molecular mobility, as diffusion within aged condensates progressively decreases with increasing β-sheet content[39–41]. Recently, the condensate's interface separating the dilute and dense phases, has emerged as a central feature controlling the behaviour of condensate biology[42]. Interfacial properties, including surface tension[43,44], zeta potential[45] or molecular adsorption[46], heavily control condensate size[47,48], stability, and interactions with cellular structures such as autophagosomes[49], microtubules[50], and endocytic pits[51]. In addition, dynamic processes including droplet coarsening, cytoskeletal organization, and cross-β-sheet stacking are modulated by the interface through its effects on molecular orientation[52] and reactivity. Consistent with this emerging view, the liquid-to-solid transition in FUS condensates has been reported by us to initiate at the droplet boundary[53,54]. Similarly, in hnRNPA1 condensates, cross-β-sheet formation during ageing occurs preferentially at the interface[40], as well as α-synuclein forms fibrils which accumulate at condensate surfaces[32,55]. Together, these observations highlight the interface as a key spatial regulator of pathological structural transitions. Hence, understanding the molecular mechanisms linking condensate morphology to ageing is essential for elucidating how aggregation is initiated, controlled in space, and ultimately connected to condensate malfunction and disease.

Computational approaches provide a powerful framework to examine the molecular mechanisms governing protein structural transitions and their spatiotemporal emergence across the condensate[56]. Here, we employ coarse-grained Molecular Dynamics (MD) simulations, both at equilibrium and non-equilibrium, to elucidate the spatial localization of inter-protein structural transitions that precipitate ageing, as well as the mechanistic factors underlying these processes[39,54]. As a proof of concept, we use a classical polymer-physics model to describe the low-complexity domain (LCD) of proteins, which provides an effective framework to explore the conformational behaviour, sequence dynamics, and phase-separation propensity. Such class of simplified models have been successfully shown to capture essential protein features, including condensate fusion times[41], protein disorder-to-order conformations[57], and sequence-dependent condensate stability[58], among others[59–61]. In our model, we define specific sites across the sequence prone to undergo structural transitions, as illustrated in Fig. 1a, which emulate low-complexity aromatic-rich kinked segments (LARKS) known to promote inter-protein β-sheet transitions[62]. We examine the spatial localization of structural transitions across the condensate as a function of sequence modifications, from purely hydrophobic sequences to amphiphilic protein LCDs. Our goal aims to identify the dominant physicochemical factors driving inter-protein structural transitions at the interfaces, as experimentally reported for FUS[53,54], hnRNPA1[40], and α-synuclein[32,55], as well as to elucidate whether this is a general mechanism independent of the protein sequence. To this end, we characterize pre- and post-ageing condensate properties including protein local density fluctuations, LCD conformational ensembles, dynamic intermolecular rearrangements, monomeric diffusion, inter-protein contact frequency maps as well as surface tension analyses as a function of sequence variations. Overall, our physics-based computational framework provides a direct connection between the spatial onset of structural transitions and the molecular mechanisms governing condensate ageing, offering mechanistic insight into how interfaces, and their associated thermodynamic and kinetic distinctions from bulk conditions, regulate protein aggregation and phase behaviour.

II. RESULTS AND DISCUSSION

A. A Minimal Low-Complexity Domain Model for Condensate Formation and Ageing

We employ an off-lattice implicit solvent protein LCD model based on the Mpipi Recharged sequence-dependent force field[63], in which each residue is represented as a spherical bead in implicit solvent (see Section S1 of the Supplementary Material, SM). Intermolecular hydrophobic interactions are approximated using the Wang–Frenkel potential[64], while chain connectivity is enforced through a bond harmonic potential. Our MD simulations are performed in LAMMPS[65] in combination with an ageing algorithm developed by us[22,39,54,66–68] that dynamically mimics intermolecular β-sheet transitions in coarse-grained protein models when multiple LARKS (i.e., structural transition sites depicted in blue; Fig. 1a) fall within a prescribed cut-off distance. Upon satisfying this distance and coordination criterion[54,67], pairwise interactions between the involved residue types are rescaled from weak, transient LCD-like contacts to strong β-sheet-like interactions, informed by all-atom calculations[39,54,67] (see Section S1 of the SM for details). To simulate phase-separation, we focus on two classes of condensate architectures: spherical droplets and

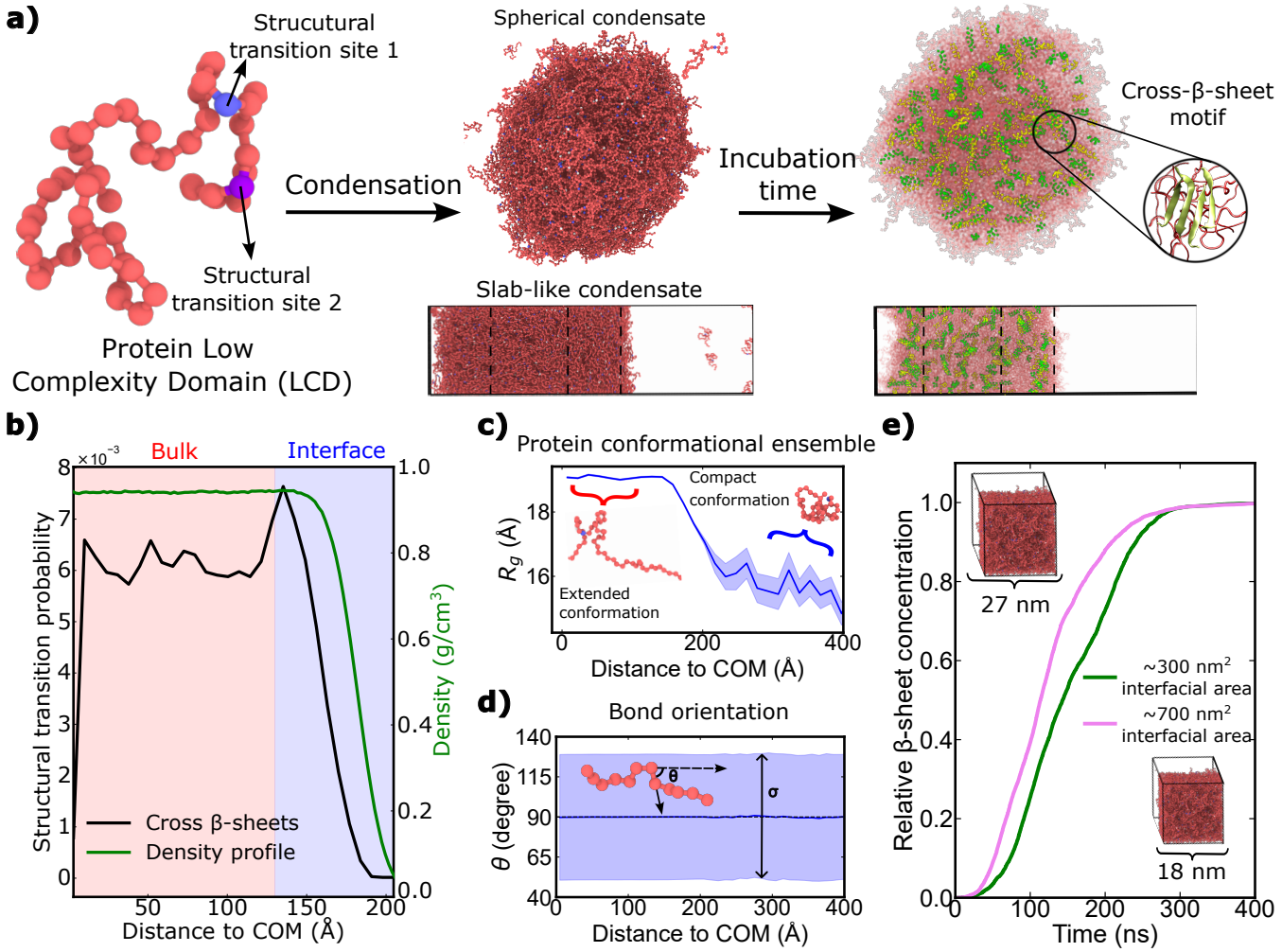

Figure 1: (a) Schematic representation of our minimal protein low-complexity domain (LCD) model which is able to undergo phase-separation and subsequent evolution, upon incubation time, into solid-like states driven by the accumulation of inter-protein β-sheets. The LCD sequence is formed by 50 homotypic residues, where beads emulating LARKS are highlighted in blue and purple. The renders depict the organization of the LCD within spherical and slab-like condensates (centre) and the cross-β-sheet structures formed over time (right). (b) Cross-β-sheet structural transition probability (black) and density profile (green) as a function of distance from the condensate centre-of-mass (COM). (c) Radius of gyration (R_g) as a function of distance from the condensate COM. Rendered images show representative conformations observed at different distances. The error is represented by a shaded region. (d) Average angle between the bond vector connecting directly linked residues and the direction normal to the interface (θ), shown as a function of distance from the condensate COM. The width of the θ distribution at each distance (σ) is indicated by the shaded region. (e) Time evolution of cross-β-sheet concentration for two condensates with different interfacial areas but constant number of LCDs. Rendered images illustrate the difference in box dimensions between both simulations to control the surface to volume ratio.

slab-like geometries, as illustrated in Fig. 1a. Slab simulations enable the calculation of phase diagrams in the temperature–concentration plane[22] (see Section SII of SM for further details), while spherical condensates, consisting of a stable droplet embedded within a cubic simulation box, permit the evaluation of high surface to volume ratios, as experimentally relevant for condensate nucleation events[69,70].

We explore the impact of LCD intermolecular interactions in condensate ageing by designing three representative sequences recapitulating small differences in the net interaction strength. The first protein LCD consists of uniform interactions along the entire sequence, corresponding to a homopolymer. The second adopts a block-copolymer architecture with a hydrophobic region characterized by enhanced intermolecular interactions and a hydrophilic region with scale-down inter-protein interactions. Finally, the third sequence follows a similar block-copolymer arrangement but with pairwise interactions tuned to accentuate the contrast

between the hydrophobic and hydrophilic segments. These amphiphilic LCDs therefore provide a more faithful approximation of real LCD phase behaviour forming biomolecular condensates and ultimately transitioning into solid-like kinetically trapped states[38].

B. Interfacial enrichment of cross-β-sheet transitions in homopolymer LCDs

We first compute the temperature–concentration phase diagram for the homopolymer LCD (hereafter referred to simply as LCD; Fig. SII) to determine the coexistence regime between condensed and dilute phases (Fig. 1a). From these simulations, using the Direct Coexistence method[71], we estimate a critical solution temperature of $T_{\mathrm{c}} = 278 \pm 2\,\mathrm{K}$. The system is then equilibrated at $T/T_{\mathrm{c}} = 0.92$, and we perform non-equilibrium simulations of condensate ageing using our dynamical algorithm[39,54], which mimics inter-protein β-sheet structural transitions when at least 4 LARKS are found in a high-density local fluctuation, inducing an enhancement of the interaction strength equivalent to those found upon a LARKS disorder-to-order transition[62,67,72]. Within these simulations, intermolecular interactions between residues capable of undergoing structural transitions (blue and purple beads in Fig. 1a) are dynamically switched over time, mimicking disorder-to-order structural transitions[62]. We characterize condensate ageing by spatially tracking through the MD trajectory the position of the spontaneous structural transitions relative to the condensate centre of mass (COM). The results, shown in Fig. 1b, reveal a pronounced maximum in the probability of structural transitions occurring near the condensate interface (black curve), averaged over ten independent simulation trajectories. While the presented data in Fig. 1b corresponds to slab-like condensates with an interfacial area of $324\,\mathrm{nm}^2$, similar trends are observed for different condensate surface to volume ratios, as well as for spherical condensates, as reported in Sections SIII and SIV of the SM.

Remarkably, we find that our minimal LCD model recapitulates the enhanced probability of structural transitions at the condensate's interface, thereby capturing a key feature experimentally reported for phase-separating RNA-binding proteins such as FUS or hnRNPA1[40,53]. Understanding the mechanistic origin of this interfacial preference is crucial for elucidating how ageing driven by cross-β-sheet transitions unfolds in biomolecular condensates. Given that our model does not incorporate chemical heterogeneities encoded across the protein sequence, we hypothesize that the observed maximum in transition probability may arise from the influence of the interface on the LCD conformational ensemble. To test this hypothesis, we analyze the LCD radius of gyration (R_g) (Fig. 1c) and bond orientation as a function of the COM distance from the condensate's core (Fig. 1d) in the pre-ageing regime (i.e., before structural transitions drive the condensate into a kinetically trapped state). The radius of gyration quantifies the overall degree of compactness of LCD proteins. Consistent with theoretical expectations and previous computational studies[60,73], we observe a monotonic decrease in R_g as the interface is approached, reflecting a gradual transition between different conformational states. LCDs within the condensate core adopt more extended conformations that maximize the intermolecular liquid network connectivity, whereas proteins in the dilute phase collapse into more compact conformations that maximize intra-LCD interactions, as reported in Fig. 1c. LCDs located across the interface display intermediate R_g values, consistent with a gradual conformational crossover.

We next examine orientational order within the protein LCDs. The bond orientation (θ) is defined as the angle between the vector connecting two consecutive beads and the unit vector normal to the interface. This metric provides insight into chain alignment and is sensitive to short-range ordering and directional sequence correlations[74,75]. When analyzed as a function of distance from the condensate COM, our simulations (Fig. 1d) reveal no preferential bond orientation, as the mean value of θ remains close to 90° at every distance. Moreover, the distribution width, quantified by σ, is essentially constant across all positions, indicating the absence of enhanced local ordering of the LCD at the interface. Together, these observations suggest that interfacial effects on single-chain orientational order are minimal. Nevertheless, when comparing ageing kinetics for condensates with different surface areas—$324\,\mathrm{nm}^2$ and $729\,\mathrm{nm}^2$—but identical total number of LCDs (Fig. 1e), we observe a markedly faster accumulation of inter-protein β-sheets in the system with larger surface to volume ratio. Figure 1e shows the time evolution of the normalized β-sheet concentration for both geometries, highlighting the speed up of condensate ageing with increasing interfacial area. These results independently confirm that the interface acts as a hotspot for structural transitions, consistent with the spatial probability profiles shown in Fig. 1b. Overall, while classical single-LCD properties such as conformational compactness and orientational order do not alone account for the preferential localization of structural transitions near the interface, the interface itself seems to play a decisive role in mediating condensate ageing. Therefore, a more comprehensive characterization is required to elucidate the mechanisms by which interfaces promote cross-β-sheet structure accumulation.

C. Enhanced mobility and intermolecular rearrangements promote ageing at the condensate interface

To further elucidate the mechanisms that govern and promote ageing at the interface, we perform a more detailed characterization of both pre-ageing and post-ageing states. We first examine monomeric mobility, quantified through short-time diffusion coefficients (see Section SX of the Supplementary Material), which provide a measure of the dynamical state of the condensate. Figure 2a presents axial-cut spatial diffusion maps before and after ageing, alongside rendered images of spherical condensates pre- and

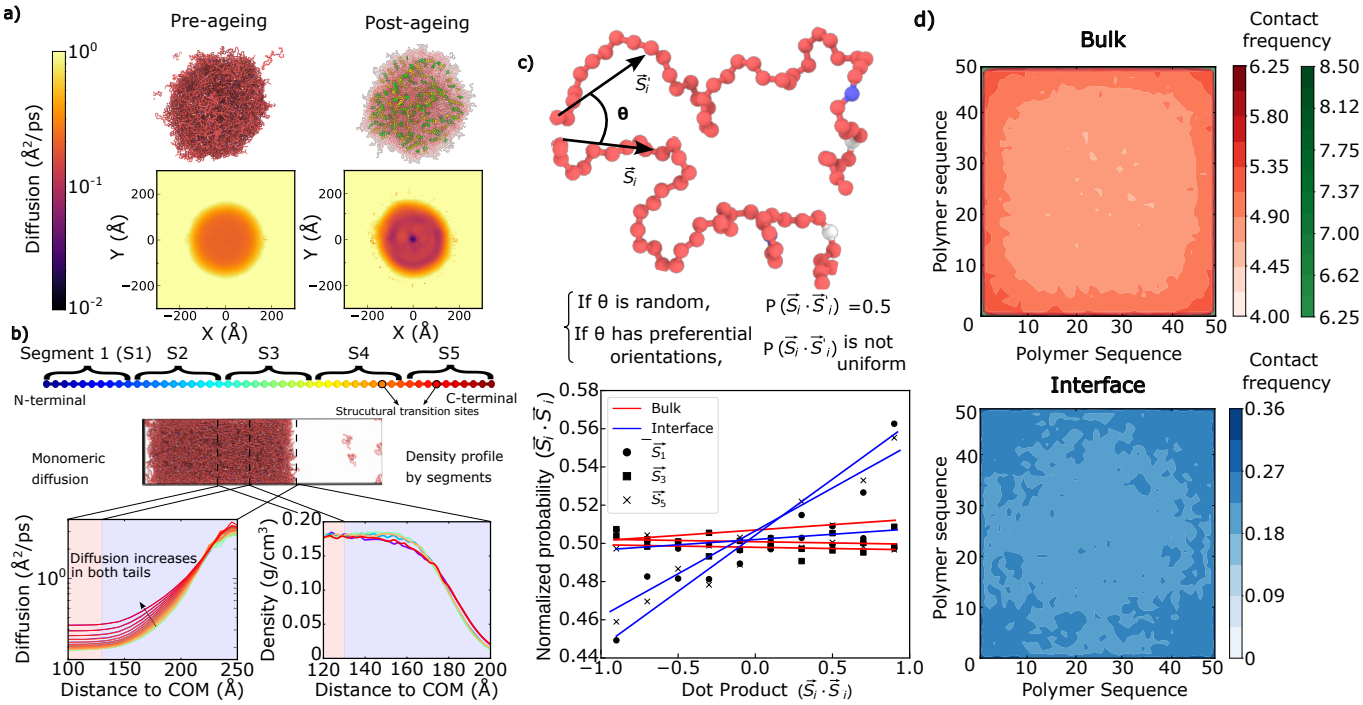

Figure 2: (a) Monomeric diffusion coefficient before (left) and after (right) ageing in spherical LCD condensates. The results are shown as projections onto the xy plane of the spherical droplet. Representative renders of the studied droplets are shown above the graphs. (b) Top: Scheme depicting the 10-residue long segments into which the sequence is classified. Middle: Render of a representative slab condensate. Bottom left: Monomeric diffusion as a function of distance from the condensate COM. Bottom right: Segment-resolved density profiles as a function of distance from the condensate COM. The plots follow the colour code shown in the top panel. (c) Normalized probability distribution of the dot product between end-to-end vectors of the same segment from different LCDs. Bulk and interface regions are considered separately, and segments S1, S3, and S5 are analysed (see panel (b) for segment definitions). A schematic representation of two LCD molecules is shown above the graph, defining the end-to-end vectors ($\vec{S}_1$) and the angle (θ). For random orientations, the normalized probability is uniform and approximately 0.5, while deviations indicate preferential intermolecular alignment. (d) Intermolecular contact frequency probability (in %) of the LCD for proteins located in the bulk and at the interface. The bulk contact map is shown using two colour scales due to the wide range of contact frequencies in this region.

post-incubation time. In the pre-ageing regime, monomers exhibit high mobility across all spatial regions. However, as condensates are incubated, LCD diffusion decreases markedly in areas where cross-β-sheet structures accumulate. While β-sheet formation is not the sole mechanism capable of reducing protein condensate mobility—density heterogeneities[76], viscoelastic effects[59], and other physicochemical processes[42,77] also contributing—it remains the dominant driver of the observed diffusion slow down in our simulations. Notably, a pronounced low-diffusion region emerges at the interface, coinciding with enhanced inter-protein β-sheet concentration. Beyond altering viscoelastic properties, reduced mobility at the interface may further limit molecular exchange between condensed and dilute phases[78,79], a mechanism central to the functional dynamics of liquid-like physiological condensates[80]. Although our diffusion analysis provides valuable insight into how ageing modifies condensate material properties—particularly molecular mobility—it does not by itself explain why the interface actively promotes structural transitions over the bulk.

Thus far, our analyses have focused on global system properties, as condensate density (Fig. 1b) or whole-chain observables, such as LCD dynamical conformation or mobility. However, to uncover the mechanisms primarily driving structural transitions at the interface, we perform a more detailed submolecular analysis. Consequently, we study monomeric mobility, measured as residue diffusion at short timescales (see Section SX of the SM), tracking the trajectory of each residue individually. In Fig. 2b (bottom left), we show the monomeric diffusion coefficient along the three directions of space as a function of the COM distance (results for the diffusion coefficient in the x-y plane and along the z direction, which yielded similar trends, are also reported in Section SX of the SM). The lines are colour-coded for each specific particle bead according to the scheme depicted in Fig. 2b (top). Interestingly, we find that terminal residues, at both ends of the LCDs, exhibit higher mobil-

ity regardless of their distance from the condensate COM. Moreover, monomeric diffusion increases for all residues as they approach the interface, with this enhancement becoming noticeable at approximately 150 Å from the condensate's centre of mass. We identify two distinct effects: (i) the inherently higher mobility of the terminal segments, independent of the location across the condensate; and (ii) an interface-induced mobility enhancement (150–170 Å, see Fig. 1b). The latter establishes an interfacial regime in which increased mobility coincides with a local density sufficient to promote intermolecular interactions. Such interplay enhances the likelihood of forming intermolecular contacts at the interface and, consequently, the probability that high-density fluctuations trigger structural transitions into cross-β-sheets. Therefore, our residue-level mobility calculations contribute to explain why the interface acts as a hotspot for condensate cross-β-sheet accumulation.

Furthermore, we analyse the condensate density profile by segmenting each protein LCD into five equal-length segments of 10 residues each. In Fig. 2b (bottom right), we show the density profile of each segment as a function of the COM distance. At the interface, (e.g., approximately 150 Å from the condensate's COM) a statistically significant difference in local density between LCD segments emerges. The terminal segments (S1 and S5) exhibit a subtle density depletion prior to the overall density drop of the condensate, but a higher relative density compared to the central segments as we approach the dilute phase (e.g., in the 180–200 Å range). This indicates that the terminal regions are preferentially located toward the interface, facing the dilute phase. In contrast, the central segments (S2, S3, and S4) maintain higher local densities at the interfacial region closer to the condensate core before undergoing a more abrupt density decay, leading to a crossover of the density probabilities within the interface. Altogether, these segmented density profiles suggest a preferential interfacial organization, in which terminal segments are enriched at the outer interface while central segments predominantly occupy a secondary coordination shell at the inner interface.

We further investigate this phenomenon by probing possible intermolecular alignment arising from the preferential arrangement of different protein segments at the interface. Specifically, we examine orientational correlations in the angle between end-to-end vectors ($\vec{S}_i$) of pairs of segments belonging to different LCDs, as defined in Fig. 2c (top). This analysis is schematically illustrated in Fig. 2c, where we report the probability distribution of the dot product between normalized end-to-end vectors of segments from different protein replicas at the condensate. In the bulk (red curves in Fig. 2c), all segments exhibit a uniform distribution, consistent with random relative orientations (i.e., a probability centred around 0.5). In contrast, at the interface (blue curves in Fig. 2c), terminal LCD segments display a pronounced orientational preference, while central segments retain the uniform distribution characteristic of isotropic alignment in bulk conditions. These results demonstrate that intermolecular orientational order emerges selectively at the interface[81] and is predominantly associated with terminal protein segments, where usually LARKS are located across the sequence[62].

Next, we perform a detailed analysis of intermolecular protein interactions by computing contact frequency maps between all sequence residues. A contact is defined as effective—i.e., ensuring a significant enthalpic gain—when two residues are separated by less than $1.2\,d$, where d denotes the molecular diameter of each residue. In Fig. 2d, we compare two distinct regions of the condensate: the bulk (red and green maps) and the interface (blue map). In both regions, we observe a clear distinction between contacts involving terminal segments and those involving central segments, with terminal regions exhibiting consistently higher contact frequencies than the middle segments. As expected, the bulk region displays a larger overall number of contacts due to its higher local density compared to the interface. To quantify the degree of heterogeneity, we examine the ratio between the minimum and maximum contact frequencies at both the interface and the core (120–140 Å and 30–50 Å distance range from the condensate's COM, respectively), displaying a more pronounced differentiation between terminal and central segments contact probability at the interface. In principle, this enhanced contrast suggests that the spatial location of the structural transition sites could influence whether cross-β-sheet formation occurs preferentially at the interface. To directly assess the magnitude of this effect, we performed additional simulations in which the structural transition sites were repositioned at the chain centre (segment S3, Fig. 2b) and analysed the resulting ageing behaviour. As shown in Section SXI of the SM, the ageing rate still exhibits a maximum near the interface. Moreover, the structural transition probability remains identical to that reported in Fig. 1b, indicating that the increased relative difference of tail–tail contacts at the interface plays a secondary role in promoting interfacial ageing as compared to enhanced monomeric diffusion, segment local clustering, and preferential alignment.

Taken together, this residue- and segment-resolved analysis demonstrates that the interface is not merely a passive boundary, but a dynamically and structurally distinct region in condensates. Terminal segments exhibit enhanced mobility, preferential localization, and orientational ordering, whereas central segments remain comparatively uniform. These trends persist even when β-sheet-prone aggregation sites are relocated, indicating that interfacial ageing emerges from the intrinsic organization and dynamics of the protein, rather than from the specific placement of the structural transition sites (e.g., LARKS in real protein sequences such as FUS, hnRNPA1, or TDP-43 among other numerous RNA-binding proteins across the human proteome[22,40,53,62]).

D. Asymmetric interaction patterning in protein sequences amplifies condensate interfacial ageing

To bridge the gap between the minimal homopolymer LCD model and the architecture of real LCDs, we next

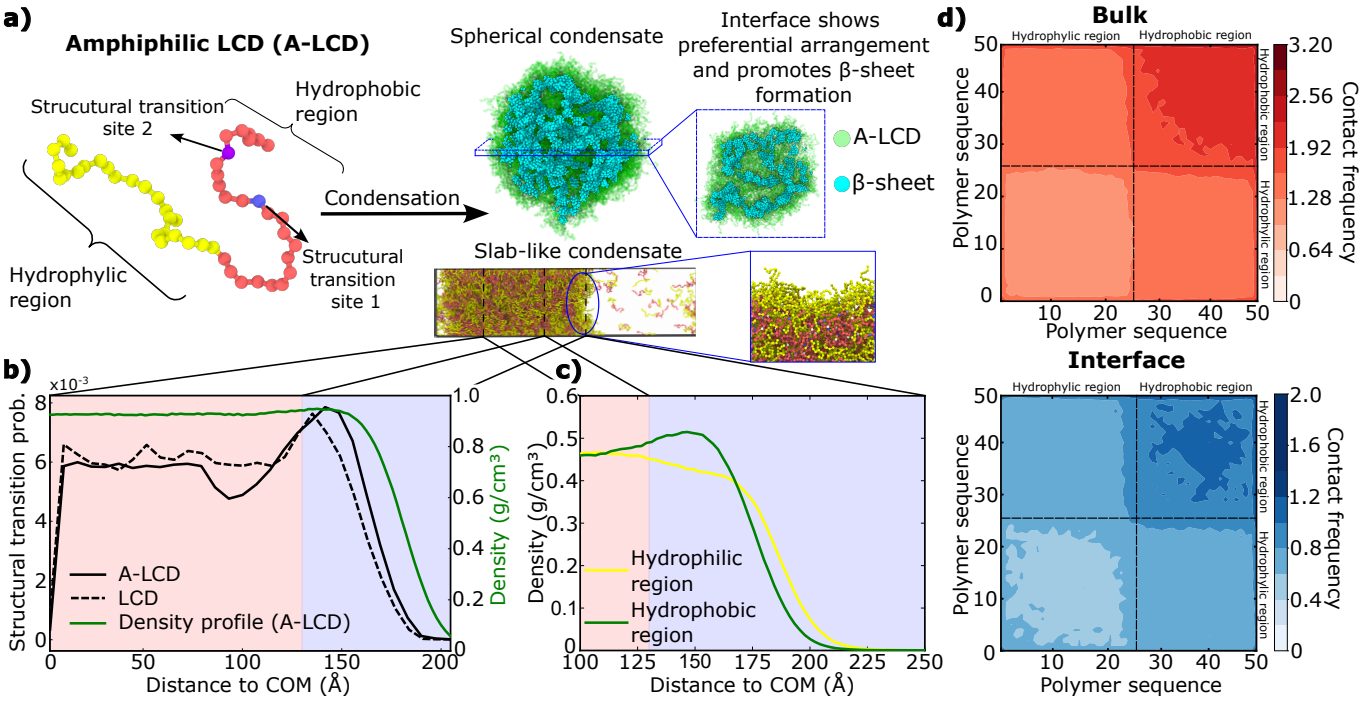

Figure 3: Amphiphilic proteins favour the appearance of β-sheet motifs at the condensate's interface. (a) Schematic representation of the condensation process of the A-LCD into spherical and slab condensates. The sequence of the A-LCD is shown on the left, highlighting the structural transition sites and the hydrophobic and hydrophilic domains. A zoomed view of the slab-like condensate illustrates the preferential arrangement of A-LCD at the interface. (b) Structural transition probability of the A-LCD (solid black line) and homopolymer LCD (dotted black line), together with the density profile of an A-LCD condensate (green), as a function of distance from the condensate COM. (c) Density profiles of the hydrophilic and hydrophobic domains of the A-LCD sequence as a function of distance from the condensate COM. (d) Intermolecular contact frequency maps (in %) of A-LCDs in bulk (top) and at the interface (bottom). The two major domains of the A-LCD are indicated by dashed lines.

introduce a more realistic protein model featuring chemically distinct regions across the sequence. As defined in Section II A, this amphiphilic LCD (A-LCD) consists of two interaction residue types, forming a more hydrophobic region with stronger intermolecular interactions, and a more hydrophilic region with weaker inter-protein interactions. A schematic representation of the A-LCD model is shown in Fig. 3a. After determining the critical solution temperature of this sequence ($T_c = 278 \pm 2$ K; see Section SII of the SM) and verifying that is almost identical to the original LCD sequence, we perform non-equilibrium condensate ageing simulations at $T/T_c = 0.92$, as before. Analogously to the homopolymer LCD model (Fig. 1), we track the cross-β-sheet accumulation across the condensate space. These results are presented in Fig. 3b, where we compare the LCD and A-LCD models, together with the corresponding density profile for an A-LCD condensate in a slab geometry. Strikingly, structural transitions are more strongly enhanced toward the interface in the A-LCD compared to the LCD sequence, exhibiting a clearer maximum in the structural transition probability. This behaviour is also evident in Fig. 3a, which shows a rendering of a spherical A-LCD condensate alongside a sliced view, revealing a preferential localization of β-sheet fibrils at the interface. Importantly, increasing the asymmetry between the hydrophobic and hydrophilic interaction strength further amplifies the interfacial maximum in structural transition probability relative to the condensate bulk (see Fig. S9 in the SM).

It is noteworthy to mention that the density profile in pre-ageing conditions, shown in Fig. 3b, exhibits a slight maximum located near the position of the peak of structural transition probability (post-ageing), a feature that is absent in the LCD density profile (Fig. 1b). To elucidate the origin of such behaviour, we decompose the density profile into contributions from the hydrophobic and hydrophilic domains. In the bulk (Fig. 3c), both regions display equivalent distributions. Upon approaching the interface, however, the two regions exhibit markedly distinct behaviours: the hydrophobic domain develops a pronounced maximum on the inner side of the interface, while the hydrophilic region decreases monotonically and undergoes a sharp drop at the boundary of the dense phase, corresponding to the portion of the protein most exposed to the dilute phase to minimize the condensate surface tension. This observation is consistent with Fig. 3a, where the rendered configurations reveal a preferential localization of hydrophilic regions at the interface, while hydrophobic regions are displaced into a secondary coordination shell within the condensate. This

spatial segregation promotes enhanced compaction through the association of hydrophobic regions, which experience stronger intermolecular interactions, thereby providing a mechanistic explanation for the emergence of a local density maximum near the interface.

To elucidate how this interfacial local density enhancement manifests at the molecular level, we examine the corresponding intermolecular contact maps of the A-LCD sequence. The contact frequency maps are shown in Fig. 3d, distinguishing between the bulk and interfacial regions of the condensate. A dashed line demarcates the hydrophobic and hydrophilic domains of the sequence in both maps. The maps reveal several key differences between the bulk and the interface. As expected, the highest contact frequencies occur within the hydrophobic region, particularly for hydrophobic–hydrophobic contacts, reflecting the stronger intermolecular interactions in this domain. In contrast, the hydrophilic region exhibits weaker and more homogeneous contact patterns, with both hydrophilic–hydrophilic and hydrophilic–hydrophobic interactions displaying lower and more uniform probabilities. Notably, the contrast between these regions becomes significantly amplified at the interface: the ratio of hydrophobic to hydrophilic-like contact frequencies increases to approximately 10:1 at the interface, compared to about 5:1 in the bulk. This enhanced disparity provides the molecular-level explanation for the strengthened interfacial structural cross-β-sheet transitions observed relative to the LCD system and directly arises from the asymmetric interaction patterning of the A-LCD sequence.

Overall, these results demonstrate that introducing chemical specificity does not substantially alter the global phase behaviour of the condensate, but it markedly influences the spatial organization of ageing within the condensate. Compared to the minimal LCD model, the A-LCD sequence produces a pronounced enhancement of structural transitions near the interface, accompanied by a peak in the density profile, driven by preferential interactions among more hydrophobic segments. Taken together, these observations indicate that asymmetric patterns of chemical interactions along the sequence reinforce the role of the interface as a structurally and dynamically distinct region that promotes ageing.

E. Surface tension minimization drives LCD alignment and enhance inter-protein structural transitions at the interface

Having established that chemical heterogeneity plays a major role in interfacial organization and the accumulation of inter-protein structural transitions, we now turn to a more comprehensive study of pre-ageing condensate properties to further investigate the factors driving enhanced structural transitions at the interface. We begin by examining the monomeric mobility of A-LCD residues, quantified through short-time diffusion coefficients (see SM Section X), to assess how molecular motion varies as a function of distance from the condensate's COM. These results are shown in Fig. 4a (bottom left), where each residue is represented by a separate curve. Compared to the homopolymer LCD (Fig. 2b), the symmetry between the two tails is lost: the hydrophilic tail exhibits higher diffusion than the hydrophobic tail. This behaviour is consistent with its lower binding network connectivity, as this region forms fewer intermolecular contacts (Fig. 2d), resulting in greater mobility. Nevertheless, this enhanced mobility alone does not explain the increased structural transitions at the interface, since the transition-prone sites are not located in this domain. In Figure S7 of the SM we present a two-dimensional analysis of monomeric mobility before and after ageing, highlighting the increased mobility at the condensate interface and its subsequent arrest following the formation of inter-protein β-sheets through the hydrophobic domain.

Besides monomeric diffusion, we also examine the condensate density profile per segment (Fig. 4a, top). The resulting profiles (Fig. 4a, bottom right) reveal a striking spatial organization within the condensate. In the bulk (not shown), all segments exhibit similar densities, consistent with a homogeneous interior. However, approaching the interface, the hydrophobic and hydrophilic segments display the same behaviour observed in Fig. 3c for the respective two major protein domains. Hydrophobic segments occupy the inner side of the interface ($\sim$150 Å), whereas more hydrophilic segments face the dilute phase at greater distances ($>$180 Å). Next, we assess whether this interfacial ordering induces intermolecular alignment by measuring the orientation of each segment using the parameter θ, as defined in Section II C. Figure 4b shows the results for the bulk (50–60 Å from the condensate COM) and interfacial regions (120–130 Å). In the bulk (red curves), all segments exhibit uniform orientation, with values centred around 0.5, reflecting the absence of directional ordering. In contrast, at the interface (blue curves), central segments display a pronounced preferential orientation, while terminal segments show a weaker, yet significant, orientational bias. We attribute the stronger orientation of central segments to their mixed hydrophobic–hydrophilic composition and their role in mediating the interfacial arrangement: aligning the hydrophobic tails at the inner interface while maintaining the hydrophilic domains at the outer layer. Overall, this analysis reveals a spatial organization distinct from the homopolymer LCD, where the chemical nature of the segments plays a more important role than their specific position along the sequence.

Lastly, we investigate how protein intermolecular arrangements at the interface—which ultimately promote structural transitions (Fig. 3)—arise from the condensate's propensity to minimize its surface tension. To test this point, we compute the interfacial free energy of pre-aged condensates (details in Section SXII of the SM) as a function of increasing protein amphiphilicity. We define the degree of amphiphilicity as the difference between the interaction strength of the hydrophobic and hydrophilic domains, expressed in terms of ε in the Wang–Frenkel potential (see Section SI of the SM). As shown in Fig. 4c, the surface tension decreases monotonically with increasing chemical sequence asymmet-

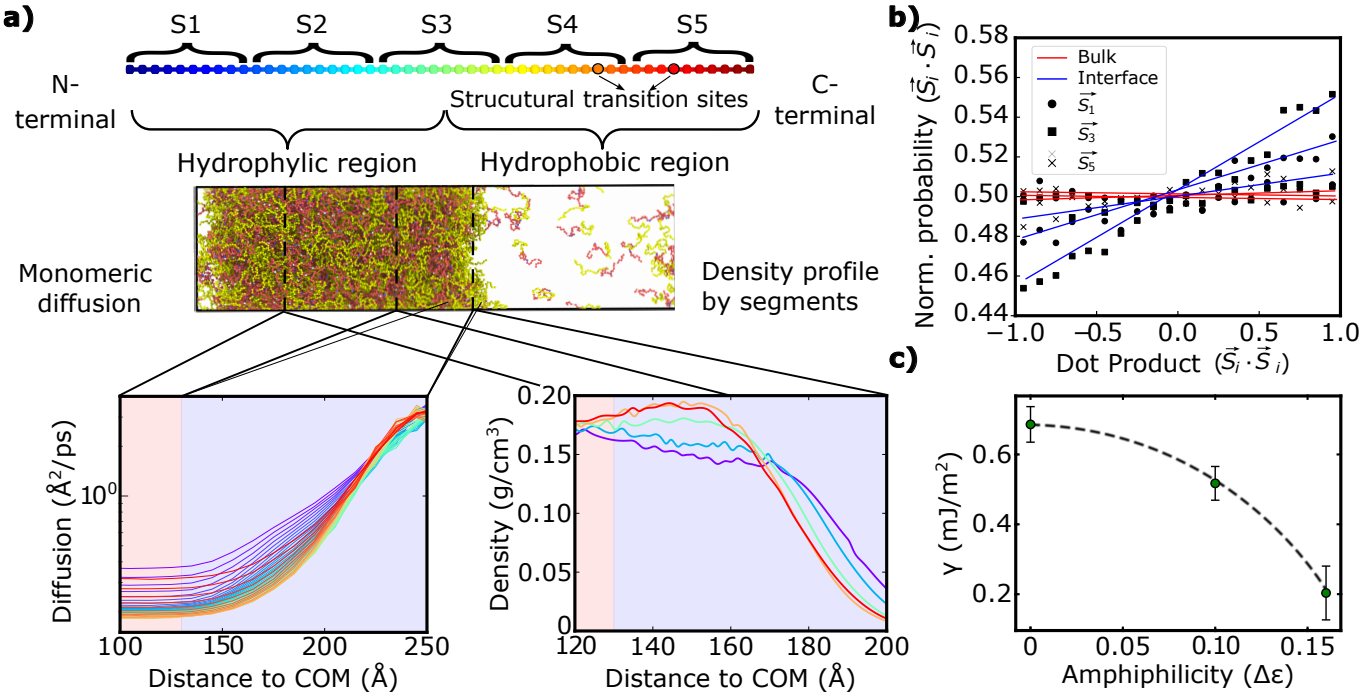

Figure 4: (a) Top: Schematic depiction of the A-LCD sequence, showing the colour code, structural transition sites, and different segments considered in our analysis. Middle: Rendered image of a representative slab simulation. Bottom left: Monomeric diffusion as a function of distance from the condensate COM. Bottom right: Segment-resolved density profiles versus distance from the condensate COM. (b) Normalized probability of the dot product between end-to-end vectors of the same segment from different LCDs. Bulk (red) and interface (blue) regions are considered separately, analysing segments S1, S3, and S5 (see panel (a) for segment definitions). Distances of 50–60 Å and 120–130 Å from the condensate COM define the bulk and interfacial regions, respectively. (c) Surface tension (γ) as a function of the amphiphilicity degree expressed in terms of the used ε value in the Wang–Frenkel potential used for describing the hydrophobic vs. hydrophilic domain interaction strength. Error bars represent standard deviation.

ric interactions. This behaviour is fully consistent with an amphiphilic organization at the interface (Figs. 3a and 4a), where the preferential orientation and clustering of chemically alike regions enable the hydrophilic domains to act as surfactants, stabilizing the interface and lowering its associated free-energy cost, in line with recent findings that sequence composition and blocky patterning modulate condensate interfacial properties[82–85].

Taken together, these results show that introducing chemical heterogeneities within the sequence leads to a condensate spatial organization distinct from that of the homopolymer LCD, further enhancing its propensity to undergo β-sheet structural transitions at the interface (Fig. 3b). The mobility profiles, segment-resolved density distributions, and orientational correlations consistently indicate that the behaviour of the A-LCD is dominated by the chemical nature of its domains rather than merely on their position along the sequence. Such organization is driven by the condensate's tendency to minimize its surface tension, which exhibits a systematic decrease with increasing chemical asymmetry without barely affecting condensate stability (Fig. S1 shows the phase diagrams of the different LCD sequences). The resulting interface, stabilized yet dynamic and chemically organized, provides a favourable environment for the emergence and localization of ageing-related structural transitions.

III. CONCLUSIONS

This study provides a detailed mechanistic understanding of how the interface of biomolecular condensates acts as a hotspot for ageing through the emergence and subsequent accumulation of inter-protein β-sheet structures. Using coarse-grained molecular dynamics simulations of a minimal protein model—mimicking low-complexity domains capable of phase-separating and further exhibiting inter-protein β-sheet transitions—we demonstrate that the interface is not merely a passive boundary, but a dynamically distinct region that promotes structural transitions. As illustrated in Fig. 5, multiple factors contribute to cross-β-sheet formation at the interface. Firstly, proteins exhibit enhanced mobility at the condensate's interface, particularly at the sequence terminal segments, which facilitates encounters between multiple protein segments capable to undergo structural transitions (Fig. 5, top left). Precisely at the interface, an interplay emerges between high protein mobility and a local protein concentration sufficient to pro-

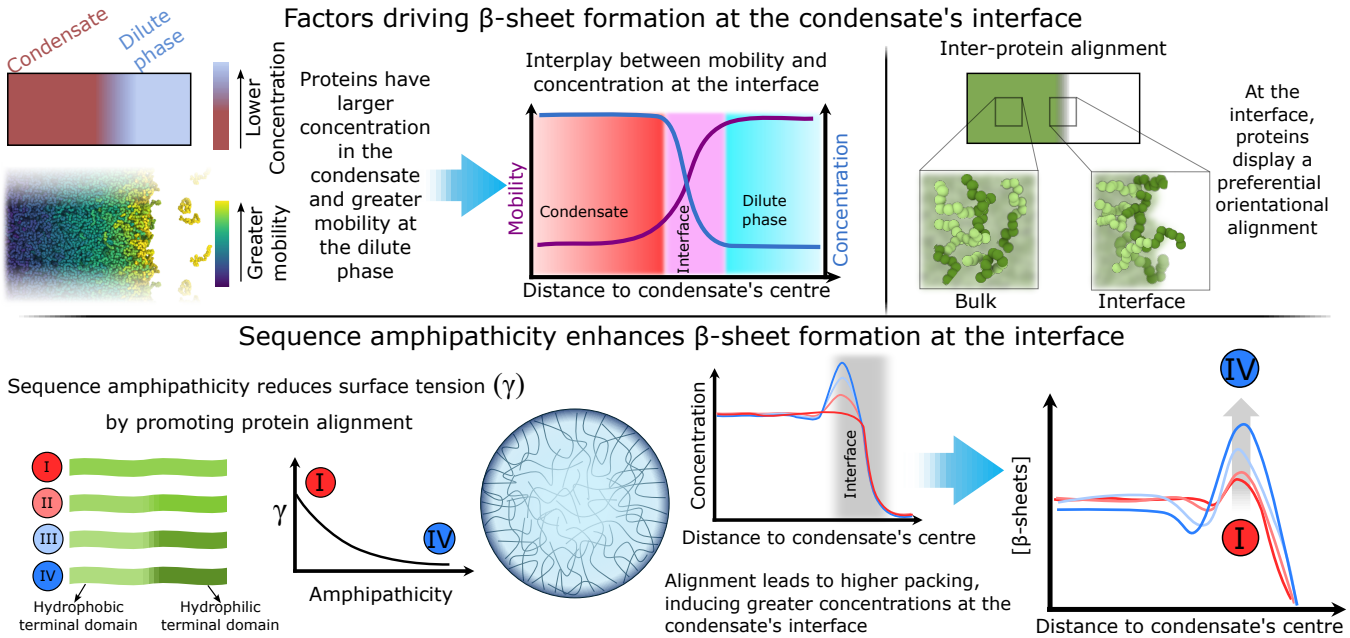

Figure 5: Top: Schematic summary of the factors contributing to the enhanced formation of inter-protein β-sheets at the condensate interface. Bottom: Schematic representation of the impact of sequence amphipathicity in condensate inter-protein β-sheet formation. The plots are illustrative.

mote cross-β-sheet transitions. Moreover, preferential inter-protein alignment between terminal domains occurs at the interface, whereas the condensate bulk exhibits a random orientational distribution of all sequence segments (Fig. 5, top right).

We find that proteins with asymmetric interactions across the sequence (e.g., A-LCD) preferentially expose their hydrophilic domains to the exterior of the condensate interface, whereas hydrophobic regions are favourably oriented toward the inner interfacial regions. Such spatial organization gives rise to a characteristic inter-protein alignment as a direct consequence of interfacial, yet dynamic ordering. The amphiphilic nature of multi-domain proteins amplify such ordering, thereby favouring inter-protein β-sheet transitions at the interface. The condensate's intrinsic tendency to minimize surface tension (Fig. 5, bottom left) further reinforces such orientational alignment, collectively maximizing enthalpic gain and minimizing interfacial free energy. Finally, as a consequence of this dynamic ordering, proteins achieve more efficient packing at the interface (Fig. 5, bottom middle), generating a maximum in density that promotes high-concentration fluctuations and the localized hardening at the condensate's interface (Fig. 5, bottom right).

Our results demonstrate that even in minimal protein models, the interface inherently favours ageing, despite the simplifications of our potential. We demonstrate how molecular asymmetric interactions within the sequence accentuate this effect by lowering surface tension and stabilizing interfacial conformations, akin to surfactant-like behaviour. Future work should investigate several aspects beyond the scope of the current study, including: (i) how longer and more complex sequences, including multi-domain proteins containing globular regions, can tune condensate interfacial hardening; (ii) how proximity to the critical point modulates surface tension and the corresponding molecular alignment at the condensate's interface; and (iii) the role of explicit water in protein dynamics and in promoting the formation of hollow condensates where most of the material is displaced toward the droplet surface upon ageing[53].

Taken together, this work underscores the interface as a central regulator of condensate ageing, with implications for understanding the spatial onset of pathological solid-like states in membraneless organelles. By linking submolecular-scale interactions to mesoscale phase behaviour, our findings provide an explanation of how general thermodynamic factors, beyond highly-specific encoded sequence features, govern the nucleation of β-sheet-rich assemblies in protein condensates, offering potential strategies to modulate or delay ageing-related processes in cellular condensates.

IV. DATA AVAILABILITY

The data that supports the findings of this study are available within the article and its Supplementary Material.

V. CODE AVAILABILITY

The necessary configuration and LAMMPS script to run a non-equilibrium ageing simulation can be found in the repository GitHub link for the repository (

https://github.com/Alex-castro-quim/Interface)

VI. ACKNOWLEDGEMENTS

I. S.-B. acknowledges funding from Derek Brewer scholarship of Emmanuel College and EPSRC Doctoral Training Programme studentship, number EP/T517847/1, Ramon y Cajal fellowship (awarded to J.R.E.), as well as the UKRI EPSRC under the UK Government's guarantee scheme (EP/Z002028/1), following successful evaluation by the ERC (Consolidator Grant awarded to R.C.G.) under the European Union's Horizon Europe research and innovation programme. A. R. T. acknowledges funding from the European Union Horizon 2020 research and innovation programme (grant agreement 803326 to R.C.-G.). J. R. E. acknowledges funding from the Ramon y Cajal fellowship (RYC2021-030937-I), the Spanish scientific plan and committee for research reference PID2022-136919NA-C33, and the European Research Council (ERC) under the under the European Union's Horizon Europe research and innovation program (grant agreement no. 101160499). A. C. and J. L. -M. acknowledge funding from the ERC grant agreement no. 101160499 (awarded to J. R. E). This work has been performed using resources provided by Archer2 (https://www.archer2.ac.uk/) funded by EPSRC Tier-2 capital grant EP/P020259/e829. The authors also thankfully acknowledge RES computational resources provided by Mare Nostrum 5 through the activity 2024-3-0001.

VII. AUTHORS CONTRIBUTIONS STATEMENT

I.S-B. and J.R.E conceived the project, and together with A.C., A.R.T., J.L-M., M.P, P.A. R.C-G, and A.O. carried it out the simulations and data analysis; J.R.E and I.S-B. supervised the project and J.R.E and R.C-G. provided computational means and funding. A.C. wrote the paper and all authors contributed equally to revising it.

VIII. COMPETING INTERESTS STATEMENT

The authors declare no competing interests

[1] M. A. Verwiel, N. A. Erkamp, and J. C. v. Hest, "Converging frontiers in biomolecular condensate and synthetic cell research," *npj Biomedical Innovations*, vol. 2, no. 1, p. 14, 2025.

[2] S. F. Banani, H. O. Lee, A. A. Hyman, and M. K. Rosen, "Biomolecular condensates: organizers of cellular biochemistry," *Nature reviews Molecular cell biology*, vol. 18, no. 5, pp. 285–298, 2017.

[3] B. Alberts, D. Bray, K. Hopkin, A. D. Johnson, J. Lewis, M. Raff, K. Roberts, and P. Walter, *Essential cell biology*. Garland Science, 2015.

[4] A. A. Hyman, C. A. Weber, and F. Jülicher, "Liquid-liquid phase separation in biology," *Annual review of cell and developmental biology*, vol. 30, no. 1, pp. 39–58, 2014.

[5] A. A. Hyman and K. Simons, "Beyond oil and water—phase transitions in cells," *Science*, vol. 337, no. 6098, pp. 1047–1049, 2012.

[6] Y. Shin and C. P. Brangwynne, "Liquid phase condensation in cell physiology and disease," *Science*, vol. 357, no. 6357, p. eaaf4382, 2017.

[7] D. S. Protter and R. Parker, "Principles and properties of stress granules," *Trends in cell biology*, vol. 26, no. 9, pp. 668–679, 2016.

[8] J. Berry, S. C. Weber, N. Vaidya, M. Haataja, and C. P. Brangwynne, "Rna transcription modulates phase transition-driven nuclear body assembly," *Proceedings of the National Academy of Sciences*, vol. 112, no. 38, pp. E5237–E5245, 2015.

[9] D. M. Mitrea, J. A. Cika, C. S. Guy, D. Ban, P. R. Banerjee, C. B. Stanley, A. Nourse, A. A. Deniz, and R. W. Kriwacki, "Nucleophosmin integrates within the nucleolus via multimodal interactions with proteins displaying r-rich linear motifs and rrna," *elife*, vol. 5, p. e13571, 2016.

[10] H. Falahati, B. Pelham-Webb, S. Blythe, and E. Wieschaus, "Nucleation by rrna dictates the precision of nucleolus assembly," *Current Biology*, vol. 26, no. 3, pp. 277–285, 2016.

[11] J. Giudice and H. Jiang, "Splicing regulation through biomolecular condensates and membraneless organelles," *Nature Reviews Molecular Cell Biology*, vol. 25, no. 9, pp. 683–700, 2024.

[12] F. Niss, L. Piñero-Paez, W. Zaidi, E. Hallberg, and A.-L. Ström, "Key modulators of the stress granule response tia1, tdp-43, and g3bp1 are altered by polyglutamine-expanded atxn7," *Molecular Neurobiology*, vol. 59, no. 8, pp. 5236–5251, 2022.

[13] J. Gal, J. Chen, D.-Y. Na, L. Tichacek, K. R. Barnett, and H. Zhu, "The acetylation of lysine-376 of g3bp1 regulates rna binding and stress granule dynamics," *Molecular and cellular biology*, vol. 39, no. 22, pp. e00052–19, 2019.

[14] W.-C. Tsai, S. Gayatri, L. C. Reineke, G. Sbardella, M. T. Bedford, and R. E. Lloyd, "Arginine demethylation of g3bp1 promotes stress granule assembly," *Journal of Biological Chemistry*, vol. 291, no. 43, pp. 22671–22685, 2016.

[15] E. W. Martin, A. S. Holehouse, I. Peran, M. Farag, J. J. Incicco, A. Bremer, C. R. Grace, A. Soranno, R. V. Pappu, and T. Mittag, "Valence and patterning of aromatic residues determine the phase behavior of prion-like domains," *Science*, vol. 367, no. 6478, pp. 694–699, 2020.

[16] S. Saha, C. A. Weber, M. Nousch, O. Adame-Arana, C. Hoege, M. Y. Hein, E. Osborne-Nishimura, J. Mahamid, M. Jahnel, L. Jawerth, *et al.*, "Polar positioning of phase-separated liquid compartments in cells regulated by an mrna competition mechanism," *Cell*, vol. 166, no. 6, pp. 1572–1584, 2016.

[17] S. Maharana, J. Wang, D. K. Papadopoulos, D. Richter, A. Pozniakovsky, I. Poser, M. Bickle, S. Rizk, J. Guillén-Boixet, T. M. Franzmann, *et al.*, "Rna buffers the phase separation behavior of prion-like rna binding proteins," *Science*, vol. 360, no. 6391, pp. 918–921, 2018.

[18] E. M. Langdon, Y. Qiu, A. Ghanbari Niaki, G. A. McLaughlin, C. A. Weidmann, T. M. Gerbich, J. A. Smith, J. M. Crutchley, C. M. Termini, K. M. Weeks, *et al.*, "mrna structure determines specificity of a polyq-driven phase separation," *Science*, vol. 360, no. 6391, pp. 922–927, 2018.

[19] M. Kato, T. W. Han, S. Xie, K. Shi, X. Du, L. C. Wu, H. Mirzaei, E. J. Goldsmith, J. Longgood, J. Pei, *et al.*, "Cell-free formation of rna granules: low complexity sequence domains form dynamic fibers within hydrogels," *Cell*, vol. 149, no. 4, pp. 753–767, 2012.

[20] T. M. Franzmann and S. Alberti, "Prion-like low-complexity sequences: Key regulators of protein solubility and phase behavior," *Journal of Biological Chemistry*, vol. 294, no. 18, pp. 7128–7136, 2019.

[21] H. Yoo, C. Triandafillou, and D. A. Drummond, "Cellular sensing by phase separation: Using the process, not just the products," *Journal of Biological Chemistry*, vol. 294, no. 18, pp. 7151–7159, 2019.

[22] N. H. Espejo, A. Feito, I. Sanchez-Burgos, A. Garaizar, M. M. Conde, A. Rey, E. Pedraza, A. Castro, R. Collepardo-Guevara, A. R. Tejedor, *et al.*, "Compositional control of aging kinetics in tdp-43 condensates," *PRX Life*, vol. 3, no. 4, p. 043018, 2025.

[23] G. Krainer, T. J. Welsh, J. A. Joseph, P. St George-Hyslop, A. A. Hyman, R. Collepardo-Guevara, S. Alberti, and T. P. Knowles, "Reentrant liquid condensate phase of proteins is stabilized by hydrophobic and non-ionic interactions," *Biophysical Journal*, vol. 120, no. 3, p. 28a, 2021.

[24] Q. Xiao, C. K. McAtee, and X. Su, "Phase separation in immune signalling," *Nature Reviews Immunology*, vol. 22, no. 3, pp. 188–199, 2022.

[25] T. M. Franzmann, M. Jahnel, A. Pozniakovsky, J. Mahamid, A. S. Holehouse, E. Nüske, D. Richter, W. Baumeister, S. W. Grill, R. V. Pappu, *et al.*, "Phase separation of a yeast prion protein promotes cellular fitness," *Science*, vol. 359, no. 6371, p. eaao5654, 2018.

[26] S. Alberti and A. A. Hyman, "Biomolecular condensates at the nexus of cellular stress, protein aggregation disease and ageing," *Nature reviews Molecular cell biology*, vol. 22, no. 3, pp. 196–213, 2021.

[27] A. S. Siebner and V. N. Uversky, "Amyloid-β, tau protein, α-synuclein, tdp-43, and fus in mixed pathology: And intrinsic disorder to rule them all," *Preprints*, 2026.

[28] W. M. Babinchak and W. K. Surewicz, "Liquid–liquid phase separation and its mechanistic role in pathological protein aggregation," *Journal of molecular biology*, vol. 432, no. 7, pp. 1910–1925, 2020.

[29] J. Li, M. Zhang, W. Ma, B. Yang, H. Lu, F. Zhou, and L. Zhang, "Post-translational modifications in liquid-liquid phase separation: a comprehensive review," *Molecular biomedicine*, vol. 3, no. 1, p. 13, 2022.

[30] M. Li, Y. Fan, Q. Li, X. Wang, L. Zhao, and M. Zhu, "Liquid-liquid phase separation promotes protein aggregation and its implications in ferroptosis in parkinson's disease dementia," *Oxidative Medicine and Cellular Longevity*, vol. 2022, no. 1, p. 7165387, 2022.

[31] C. J. Webber, S. E. Lei, and B. Wolozin, "The pathophysiology of neurodegenerative disease: Disturbing the balance between phase separation and irreversible aggregation," *Progress in molecular biology and translational science*, vol. 174, pp. 187–223, 2020.

[32] W. P. Lipiński, B. S. Visser, I. Robu, M. A. Fakhree, S. Lindhoud, M. M. Claessens, and E. Spruijt, "Biomolecular condensates can both accelerate and suppress aggregation of α-synuclein," *Science advances*, vol. 8, no. 48, p. eabq6495, 2022.

[33] S. Wegmann, B. Eftekharzadeh, K. Tepper, K. M. Zoltowska, R. E. Bennett, S. Dujardin, P. R. Laskowski, D. MacKenzie, T. Kamath, C. Commins, *et al.*, "Tau protein liquid–liquid phase separation can initiate tau aggregation," *The EMBO journal*, vol. 37, no. 7, p. e98049, 2018.

[34] R. E. Tato, A. Frank, and A. Hernanz, "Tau protein concentrations in cerebrospinal fluid of patients with dementia of the alzheimer type.," *Journal of Neurology, Neurosurgery & Psychiatry*, vol. 59, no. 3, pp. 280–283, 1995.

[35] M. Von Bergen, S. Barghorn, L. Li, A. Marx, J. Biernat, E.-M. Mandelkow, and E. Mandelkow, "Mutations of tau protein in frontotemporal dementia promote aggregation of paired helical filaments by enhancing local β-structure," *Journal of Biological Chemistry*, vol. 276, no. 51, pp. 48165–48174, 2001.

[36] A. J. Espay, A. Sturchio, A. Imarisio, E. J. Hill, B. Williamson, K. Montemagno, C. Hoffmann, H. L. Roy, D. Milovanovic, and F. P. Manfredsson, "Physics of protein aggregation in normal and accelerated brain aging," *BioEssays*, p. e70030, 2025.

[37] M. N. Starodubtseva, "Mechanical properties of cells and ageing," *Ageing research reviews*, vol. 10, no. 1, pp. 16–25, 2011.

[38] I. Alshareedah, W. M. Borcherds, S. R. Cohen, A. Singh, A. E. Posey, M. Farag, A. Bremer, G. W. Strout, D. T. Tomares, R. V. Pappu, *et al.*, "Sequence-specific interactions determine viscoelasticity and ageing dynamics of protein condensates," *Nature Physics*, vol. 20, no. 9, pp. 1482–1491, 2024.

[39] A. R. Tejedor, I. Sanchez-Burgos, M. Estevez-Espinosa, A. Garaizar, R. Collepardo-Guevara, J. Ramirez, and J. R. Espinosa, "Protein structural transitions critically transform the network connectivity and viscoelasticity of rna-binding protein condensates but rna can prevent it," *Nature communications*, vol. 13, no. 1, p. 5717, 2022.

[40] M. Linsenmeier, L. Faltova, C. Morelli, U. Capasso Palmiero, C. Seiffert, A. M. Küffner, D. Pinotsi, J. Zhou, R. Mezzenga, and P. Arosio, "The interface of condensates of the hnrnpa1 low-complexity domain promotes formation of amyloid fibrils," *Nature chemistry*, vol. 15, no. 10, pp. 1340–1349, 2023.

[41] N. A. Erkamp, I. Sanchez-Burgos, A. Zhou, T. J. Krug, S. Qamar, T. Sneideris, E. Zhang, K. Nakajima, A. Chen, R. Collepardo-Guevara, *et al.*, "Dynamically arrested condensate fusion creates complex structures with varying material properties," *bioRxiv*, pp. 2024–11, 2024.

[42] H. Wang and Z. Shi, "The rheology and interfacial properties of biomolecular condensates," *Biophysical Reviews*, pp. 1–25, 2025.

[43] J. Qin, D. Priftis, R. Farina, S. L. Perry, L. Leon, J. Whitmer, K. Hoffmann, M. Tirrell, and J. J. De Pablo, "Interfacial tension of polyelectrolyte complex coacervate phases," *ACS Macro Letters*, vol. 3, no. 6, pp. 565–568, 2014.

[44] D. M. Mitrea, B. Chandra, M. C. Ferrolino, E. B. Gibbs, M. Tolbert, M. R. White, and R. W. Kriwacki, "Methods for physical characterization of phase-separated bodies and membrane-less organelles," *Journal of molecular biology*, vol. 430, no. 23, pp. 4773–4805, 2018.

[45] T. J. Welsh, G. Krainer, J. R. Espinosa, J. A. Joseph, A. Sridhar, M. Jahnel, W. E. Arter, K. L. Saar, S. Alberti, R. Collepardo-Guevara, *et al.*, "Surface electrostatics govern the emulsion stability of biomolecular condensates," *Nano*

letters, vol. 22, no. 2, pp. 612–621, 2022.

[46] N. A. Erkamp, M. Farag, Y. Qiu, D. Qian, T. Sneideris, T. Wu, T. J. Welsh, H. Ausserwöger, T. J. Krug, G. Chauhan, *et al.*, "Differential interactions determine anisotropies at interfaces of rna-based biomolecular condensates," *Nature communications*, vol. 16, no. 1, p. 3463, 2025.

[47] I. Sanchez-Burgos, J. A. Joseph, R. Collepardo-Guevara, and J. R. Espinosa, "Size conservation emerges spontaneously in biomolecular condensates formed by scaffolds and surfactant clients," *Scientific Reports*, vol. 11, no. 1, p. 15241, 2021.

[48] F. Dar and R. Pappu, "Restricting the sizes of condensates," *Elife*, vol. 9, p. e59663, 2020.

[49] J. Agudo-Canalejo, S. W. Schultz, H. Chino, S. M. Migliano, C. Saito, I. Koyama-Honda, H. Stenmark, A. Brech, A. I. May, N. Mizushima, *et al.*, "Wetting regulates autophagy of phase-separated compartments and the cytosol," *Nature*, vol. 591, no. 7848, pp. 142–146, 2021.

[50] F. Yang, M. Ding, X. Song, F. Chen, T. Yang, C. Wang, C. Hu, Q. Hu, Y. Yao, S. Du, *et al.*, "Organization of microtubule plus-end dynamics by phase separation in mitosis," *Journal of Molecular Cell Biology*, vol. 16, no. 2, p. mjae006, 2024.

[51] J. M. Dragwidge, Y. Wang, L. Brocard, A. De Meyer, R. Hudeček, D. Eeckhout, P. Grones, M. Buridan, C. Chambaud, P. Pejchar, *et al.*, "Biomolecular condensation orchestrates clathrin-mediated endocytosis in plants," *Nature Cell Biology*, vol. 26, no. 3, pp. 438–449, 2024.

[52] D. J. Bauer and A. Nikoubashman, "The conformations of protein chains at the interface of biomolecular condensates," *Nature Communications*, vol. 15, no. 1, p. 9975, 2024.

[53] Y. Shen, A. Chen, W. Wang, Y. Shen, F. S. Ruggeri, S. Aime, Z. Wang, S. Qamar, J. R. Espinosa, A. Garaizar, *et al.*, "The liquid-to-solid transition of fus is promoted by the condensate surface," *Proceedings of the National Academy of Sciences*, vol. 120, no. 33, p. e2301366120, 2023.

[54] A. Garaizar, J. R. Espinosa, J. A. Joseph, G. Krainer, Y. Shen, T. P. Knowles, and R. Collepardo-Guevara, "Aging can transform single-component protein condensates into multiphase architectures," *Proceedings of the National Academy of Sciences*, vol. 119, no. 26, p. e2119800119, 2022.

[55] R. J. Thrush, D. M. Vadukul, S. C. Allerton, M. Storch, and F. A. Aprile, "Surface wetting is a key determinant of α-synuclein condensate maturation," *Communications Chemistry*, vol. 8, no. 1, p. 379, 2025.

[56] Y. Shan, C.-L. Ren, and Y.-Q. Ma, "Protein aging dynamics: A perspective from non-equilibrium coarse-grained models," *Chinese Physics B*, vol. 34, no. 5, p. 058301, 2025.

[57] A. Garaizar, I. Sanchez-Burgos, R. Collepardo-Guevara, and J. R. Espinosa, "Expansion of intrinsically disordered proteins increases the range of stability of liquid–liquid phase separation," *Molecules*, vol. 25, no. 20, p. 4705, 2020.

[58] A. Statt, H. Casademunt, C. P. Brangwynne, and A. Z. Panagiotopoulos, "Model for disordered proteins with strongly sequence-dependent liquid phase behavior," *The Journal of chemical physics*, vol. 152, no. 7, 2020.

[59] F. Watanabe, T. Akimoto, R. B. Best, K. Lindorff-Larsen, R. Metzler, and E. Yamamoto, "Diffusion of intrinsically disordered proteins within protein condensates," *Physical Review Research*, vol. 7, no. 4, p. 043117, 2025.

[60] J. Wang, D. S. Devarajan, A. Nikoubashman, and J. Mittal, "Conformational properties of polymers at droplet interfaces as model systems for disordered proteins," *ACS Macro Letters*, vol. 12, no. 11, pp. 1472–1478, 2023.

[61] S. Rekhi, D. Sundaravadivelu Devarajan, M. P. Howard, Y. C. Kim, A. Nikoubashman, and J. Mittal, "Role of strong localized vs weak distributed interactions in disordered protein phase separation," *The Journal of Physical Chemistry B*, vol. 127, no. 17, pp. 3829–3838, 2023.

[62] M. P. Hughes, M. R. Sawaya, D. R. Boyer, L. Goldschmidt, J. A. Rodriguez, D. Cascio, L. Chong, T. Gonen, and D. S. Eisenberg, "Atomic structures of low-complexity protein segments reveal kinked β sheets that assemble networks," *Science*, vol. 359, no. 6376, pp. 698–701, 2018.

[63] A. R. Tejedor, A. Aguirre Gonzalez, M. J. Maristany, P. Y. Chew, K. Russell, J. Ramirez, J. R. Espinosa, and R. Collepardo-Guevara, "Chemically informed coarse-graining of electrostatic forces in charge-rich biomolecular condensates," *ACS Central Science*, vol. 11, no. 2, pp. 302–321, 2025.

[64] X. Wang, S. Ramírez-Hinestrosa, J. Dobnikar, and D. Frenkel, "The lennard-jones potential: when (not) to use it," *Physical Chemistry Chemical Physics*, vol. 22, no. 19, pp. 10624–10633, 2020.

[65] S. Plimpton, "Fast parallel algorithms for short-range molecular dynamics," *Journal of computational physics*, vol. 117, no. 1, pp. 1–19, 1995.

[66] I. Sanchez-Burgos, A. R. Tejedor, A. Castro, A. Feito, R. Collepardo-Guevara, and J. R. Espinosa, "Charged peptides enriched in aromatic residues decelerate condensate ageing driven by cross-β-sheet formation," *Nature Communications*, vol. 16, no. 1, p. 8050, 2025.

[67] S. Blazquez, I. Sanchez-Burgos, J. Ramirez, T. Higginbotham, M. M. Conde, R. Collepardo-Guevara, A. R. Tejedor, and J. R. Espinosa, "Location and concentration of aromatic-rich segments dictates the percolating intermolecular network and viscoelastic properties of ageing condensates," *Advanced Science*, vol. 10, no. 25, p. 2207742, 2023.

[68] E. Pedraza, D. Hoyos, A. Feito, F. Gámez, I. Sanchez-Burgos, R. Collepardo-Guevara, A. R. Tejedor, and J. R. Espinosa, "Charged mutations in the fus low-complexity domain modulate condensate aging kinetics," *Cell Reports Physical Science*, vol. 6, no. 9, 2025.

[69] L. Li, M. Paloni, A. R. Finney, A. Barducci, and M. Salvalaglio, "Nucleation of biomolecular condensates from finite-sized simulations," *The Journal of Physical Chemistry Letters*, vol. 14, no. 7, pp. 1748–1755, 2023.

[70] S. F. Shimobayashi, P. Ronceray, D. W. Sanders, M. P. Haataja, and C. P. Brangwynne, "Nucleation landscape of biomolecular condensates," *Nature*, vol. 599, no. 7885, pp. 503–506, 2021.

[71] J. R. Espinosa, J. A. Joseph, I. Sanchez-Burgos, A. Garaizar, D. Frenkel, and R. Collepardo-Guevara, "Liquid network connectivity regulates the stability and composition of biomolecular condensates with many components," *Proceedings of the National Academy of Sciences*, vol. 117, no. 24, pp. 13238–13247, 2020.

[72] A. Šarić, Y. C. Chebaro, T. P. Knowles, and D. Frenkel, "Crucial role of nonspecific interactions in amyloid nucleation," *Proceedings of the National Academy of Sciences*, vol. 111, no. 50, pp. 17869–17874, 2014.

[73] P. J. Flory and M. Volkenstein, "Statistical mechanics of chain molecules," 1969.

[74] H. Tanaka, "Bond orientational order in liquids: Towards a unified description of water-like anomalies, liquid-liquid transition, glass transition, and crystallization: Bond orientational order in liquids," *The European Physical Journal E*, vol. 35, no. 10, p. 113, 2012.

[75] S. Fujiwara and T. Sato, "Molecular dynamics simulations of structural formation of a single polymer chain: Bond-orientational order and conformational defects," *The Journal of chemical physics*, vol. 107, no. 2, pp. 613–622, 1997.

[76] J. Wang, J.-M. Choi, A. S. Holehouse, H. O. Lee, X. Zhang, M. Jahnel, S. Maharana, R. Lemaitre, A. Pozniakovsky, D. Drechsel, *et al.*, "A molecular grammar governing the driving forces for phase separation of prion-like rna binding proteins," *Cell*, vol. 174, no. 3, pp. 688–699, 2018.

[77] Y. Kanakubo, C. Watanabe, J. Yamamoto, N. Yanagisawa, H. Sakuta, A. Nikoubashman, and M. Yanagisawa, "Cell-sized confinements alter molecular diffusion in concentrated polymer solutions due to length-dependent wetting of polymers," *ACS Materials Au*, vol. 3, no. 5, pp. 442–449, 2023.

[78] I. Sanchez-Burgos, J. R. Espinosa, J. A. Joseph, and R. Collepardo-Guevara, "Valency and binding affinity variations can regulate the multilayered organization of protein condensates with many components," *Biomolecules*, vol. 11, no. 2, p. 278, 2021.

[79] S. Weidtkamp-Peters, T. Lenser, D. Negorev, N. Gerstner, T. G. Hofmann, G. Schwanitz, C. Hoischen, G. Maul, P. Dittrich, and P. Hemmerich, "Dynamics of component exchange at pml nuclear bodies," *Journal of cell science*, vol. 121, no. 16, pp. 2731–2743, 2008.

[80] Y. Zhang, A. G. Pyo, R. Kliegman, Y. Jiang, C. P. Brangwynne, H. A. Stone, and N. S. Wingreen, "The exchange dynamics of biomolecular condensates," *Elife*, vol. 12, p. RP91680, 2024.

[81] A. P. Latham, L. Zhu, D. A. Sharon, S. Ye, A. P. Willard, X. Zhang, and B. Zhang, "Microphase separation produces interfacial environment within diblock biomolecular condensates," *Elife*, vol. 12, p. RP90750, 2025.

[82] B. Favetta, H. Wang, Z. Shi, and B. S. Schuster, "Amphiphilic protein surfactants reduce the interfacial tension of biomolecular condensates," *Langmuir*, vol. 41, no. 35, pp. 23827–23836, 2025.

[83] A. Vasquez-Briceno, G. R. Perez-Lemus, J. C. Armas-Perez, and A. Ramírez-Hernández, "Multiblock copolymers at liquid–liquid interfaces: Effect of the block sequence on interfacial tension and polymer conformation," *The Journal of Physical Chemistry B*, vol. 129, no. 11, pp. 3041–3052, 2025.

[84] T. N. Schneider, F. Stoffel, M. A. Bühler, K. Mrzilkova, M. Radiom, and P. Arosio, "Engineering nanocondensate formation through sequence composition and patterning," *bioRxiv*, pp. 2026–02, 2026.

[85] T. N. Schneider, M. Gil-Garcia, M. A. Bühler, L. F. Santos, L. Faltova, G. Guillén-Gosálbez, and P. Arosio, "De novo design of peptides localizing at the interface of biomolecular condensates," *bioRxiv*, pp. 2025–05, 2025.